Eur. Phys. J. A (2022) 58:225
https://doi.org/10.1140/epja/s10050-022-00882-9

THE EUROPEAN PHYSICAL JOURNAL A

Regular Article - Theoretical Physics

An improved unified formula for α-decay and cluster radioactivity of heavy and superheavy nuclei

M. Ismail, A. Y. Ellithi, A. Adel[a], M. A. Abbas

Physics Department, Faculty of Science, Cairo University, Giza 12613, Egypt

Received: 27 August 2022 / Accepted: 2 November 2022

Communicated by Chong Qi

Abstract Improved NRDX empirical formula for α- and cluster decay half-lives is modified by adding the effects of angular momentum, isospin asymmetry and parity. The coefficients are determined using the latest experimental data for α-decay half-lives of 573 nuclei and the available 22 cluster decay half-lives. The modified formulas produced the α- and cluster decay half-lives and agree with calculations of other similar formulas. We used the new formulas to calculate the half-lives of cluster emissions of the SHN with $Z = 120$, 122, 124, and 126, which have not yet been experimentally synthesized.

1 Introduction

The study of superheavy nuclei (SHN), having $Z \geq 104$, and the quest for an "island of stability" have become a topic of active research over the past several decades [1–18]. These SHN owe their existence to stabilizing nuclear shell effects [9,12,19]. They were synthesized by heavy-ion fusion reactions using two fusion evaporation mechanisms. The first approach is the cold fusion reactions employing ^{208}Pb or ^{209}Bi targets with various projectiles, such method is adopted at GSI (Darmstadt) and RIKEN (Wako) [14,20]. The second mechanism is the hot fusion reactions using doubly magical neutron-rich ^{48}Ca projectiles striking actinide targets which have been successfully carried out to synthesize SHN with $Z = 112 - 118$ at various research laboratories such as JINR-FLNR (Dubna), and LBNL (Berkeley) [9,12,13,21]. A continuing competition towards synthesizing ever heavier elements beyond Og is still ongoing [22–24].

Superheavy nuclei decay mainly by α-decay [4,12,25,26]. The investigation of α-decay chains, which are typically followed by spontaneous fission, are the main mechanism by which SHN could be identified [12,17,18]. In addition to these dominant decay modes, Poenaru et al. [27–29] had predicted regions in superheavy nuclei where cluster radioactivity will dominate.

Several theoretical approaches were put forth to explain the cluster radioactivity [30–32]. These models can generally be classified into two groups: fission-like and cluster-like models. In the fission like approach [29,33], the nucleus continuously undergoes deformation as a series of geometrical shapes and the cluster is considered to be formed gradually during the adiabatic rearrangements of parent nuclei till the scission configuration is reached. For the cluster-like model, which is considered a nonadiabatic method and it is comparable to the α-decay approach, in which the cluster is preformed having a certain preformation probability in the decaying parent nucleus then it penetrates through the Coulomb barrier [30,34]. Several theoretical approaches have been developed to successfully describe α-decay and cluster radioactivity such as the generalized liquid-drop model [35,36], the density-dependent cluster model [4,26,30,34,37,38], the fission-like model [28,29,39], and the Coulomb and Proximity potential model (CPPM) [7,8,40,41].

A fully microscopic treatment of α-decay and cluster radioactivity is a complex and difficult quantum-mechanical problem. A number of microscopic models have been developed over the past century for describing these decay processes. Qi et al. [42] have provided a review on a recent developments of radioactive particle decay process with recent experimental and theoretical progress in this field. Warda et al. [43] have investigated from a microscopic perspective the cluster emission properties of a wide range of even-even actinide nuclei from ^{222}Ra to ^{242}Cm using the mean-field Hartree–Fock–Bogoliubov theory with the phenomenological Gogny interaction. Mercier et al. [44] have performed a microscopic calculation of half-lives to analyze the recently observed α-decay chain $^{108}\text{Xe} \rightarrow {}^{104}\text{Te} \rightarrow {}^{100}\text{Sn}$ using a self-consistent framework based on energy density function-

[a] e-mail: ahmedadel@sci.cu.edu.eg (corresponding author)

Published online: 17 November 2022

als. Mirea [45] studied microscopically the α-decay half-lives and the fine structure phenomenon with fission-like models by solving time-dependent pairing equations. Xu et al. [46] presented a microscopic calculation of α-cluster formation in heavy nuclei by using the quartetting wave function approach (QWFA) inspired by the successful application of the THSR (Tohsaki–Horiuchi–Schuck-Röpke) wavefunction concept to light nuclei. By using the QWFA, Yang et al. [47] presented a microscopic calculation of α-cluster formation and decay in ^{104}Te, ^{212}Po, and their neighbors. Recently, Yang et al. [48] studied shell structure effects on α-cluster formation and decay by using the quartetting wave function approach (QWFA). They found that both the α-cluster formation probability and the half-life are sensitive to the quartet shell model states. Recently, Uzawa et al. [49] examined the applicability of the generator coordinate method (GCM) as a microscopic theory for cluster radioactivity of heavy nuclei. This microscopic approach can be viewed as fission with large mass asymmetry, i.e. a phenomenon between fission and α-decays.

Numerous analytical and empirical formulas are suggested to predict the half-lives of these two decay modes [2,50–56]. Many of these formulas undergo periodic modifications in various forms to fit the most recent experimental data. For example, Sahu et al. [57] derived a semi-empirical relationship for computing decay half-lives of the emission of positively charged particles like cluster, α and proton carrying orbital angular momenta based on the Coulomb scattering of resonance phenomenon of a system composed of emitted particle and residual daughter nucleus. An improved Sahu (ImSahu) semi-empirical relationship has been developed for α-decay half-lives by introducing a precise charge radius formula and an analytic expression for preformation probability [58]. Recently, on the same basis another improved formula has been suggested for cluster radioactivity [59]. Poenaru et al. [60] derived a single universal curve for both α-decay and cluster radioactivity. Qi et al. [61,62] derived the UDL formula starting from the microscopic mechanism of the charged-particle emission. Qi et al. [63] have considered the influence of the centrifugal barrier on the half-lives of proton decay by using the UDL formula including ℓ-term. The universal decay law (UDL) has been modified to take into account the isospin effects and this form has called as the modified universal decay law (MUDL) by Akrawy et al. [53]. Recently, Soylu and Qi [50] have modified UDL formula in order to consider the angular momentum including parity and isospin effects for both α and cluster decays. Ren et al. [64] developed an empirical formula between the half-lives and decay energies of cluster radioactivity which is a natural generalization of the Geiger–Nuttall law and Viola–Seaborg formula from simple α decay to complex cluster radioactivity. This formula was modified a few years later in 2008 by Ni et al. [65] by including the reduced mass term using the WKB approximation to develop an empirical formula (NRDX formula) for half-lives of both α-decay and cluster radioactivity.

In our previous work [2], we started by Royer's formula for α-decay half-lives and derived five improved empirical formulas that can be used to calculate α-decay half-lives of heavy and superheavy nuclei. In the present work, we extend our previous study to include cluster radioactivity. For this purpose, we modify NRDX formula for both α-decay and cluster radioactivity by considering the contribution of the orbital angular momentum, isospin asymmetry, and parity effects. The coefficients of the improved formulas for even-even, even-odd, odd-even and odd-odd nuclei are fitted using the latest evaluated half-lives over a wide range of 573 nuclei between $52 \leq Z \leq 118$. Moreover, the shell closures are systematically investigated and correlated with the neutron number variation of logarithmic half-lives $\log T$. The predictions of half-lives for both α-decay and cluster radioactivity in the uncharted territory of superheavy nuclei are presented using the improved modified formula.

2 Theoretical framework

2.1 NRDX formula without any modifications (Formula-A)

From the WKB barrier penetration probability, Ni et al. [65] proposed an analytical formula (NRDX formula) for half lives and decay energies for α decay and cluster radioactivity as:

$$\log_{10} T_{1/2} = a\sqrt{\mu}\, Z_c\, Z_d\, Q_c^{-1/2} + b\sqrt{\mu}\,(Z_c\, Z_d)^{1/2} + c, \quad (1)$$

where Z_c and Z_d are the atomic numbers of the cluster, and daughter nuclei, respectively, while Q_c is the decay energy of the cluster. $\mu$is the reduced mass of the cluster-daughter system measured in unit of the nucleon mass, $\mu = A_c A_d/(A_c + A_d)$. The parameters a, b and c are determined by fitting to the experimental data for all different sets. Their original values were developed via fitting experimentally data of 262 nuclei listed in [65].

We updated these parameters, reported in Table 1, by fitting to the recent available experimental data over a wide range of 573 nuclei ($52 \leq Z \leq 118$). The parity and spin assignments of parent and daughter nuclei together with the experimental α-decay half-lives are obtained from NUBASE2020 [66]. The experimental Q_c is extracted from the most recent AME2020 atomic mass evaluation [67],

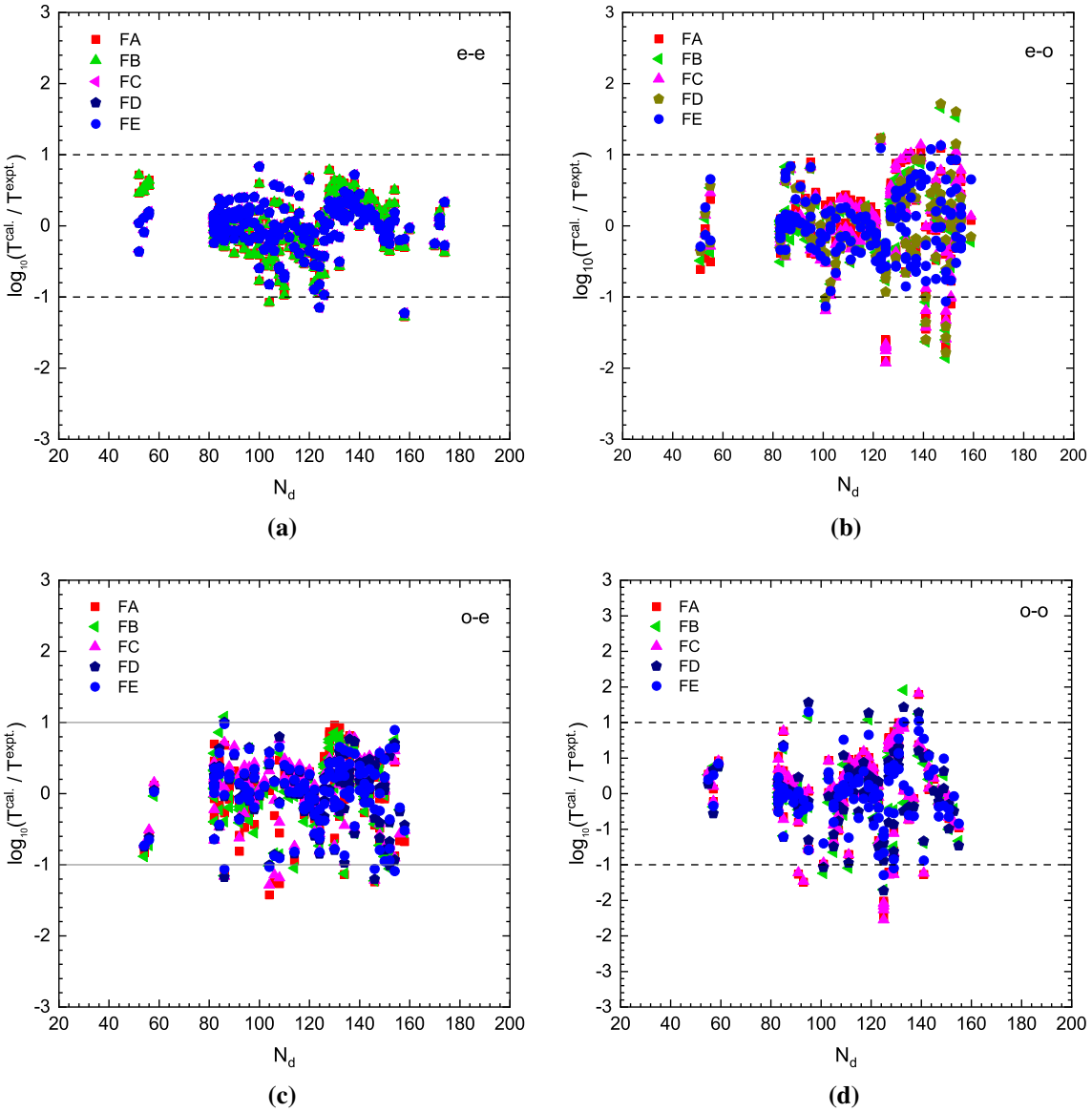

Fig. 1 Deviation of the calculated and experimental α-decay half-lives for the four categories of nuclei (e–e, e–o, o–e, o–o) using the five formulas given by Eqs. (1), (2), (4), (5), and (6) against the neutron number, N_d, of daughter nuclei

Table 1 The parameters of proposed FA for all sets of α emitters

Set	a	b	c
e–e	0.402453	− 1.48927	− 12.29808
e–o	0.408676	− 1.38023	− 15.34091
o–e	0.409329	− 1.46321	− 13.40666
o–o	0.419935	− 1.41320	− 15.55893
All nuclei	0.403295	− 1.427378	− 13.58144

2.2 NRDX formula including ℓ-angular momentum (Formula-B)

Taking into consideration the impact of the centrifugal potential, the improved formula is written as:

$$\log_{10} T_{1/2} = a\sqrt{\mu}\, Z_c\, Z_d\, Q_c^{-1/2} + b\sqrt{\mu}\,(Z_c\, Z_d)^{1/2} + c + d\,\ell(\ell+1), \quad (2)$$

where the original NRDX formula's first three terms are the same.The centrifugal potential is represented by the fourth term. ℓ is the angular momentum taken away by the cluster. The minimal angular momentum (ℓ_{min}) that the cluster takes away can be calculated using the conservation rules for

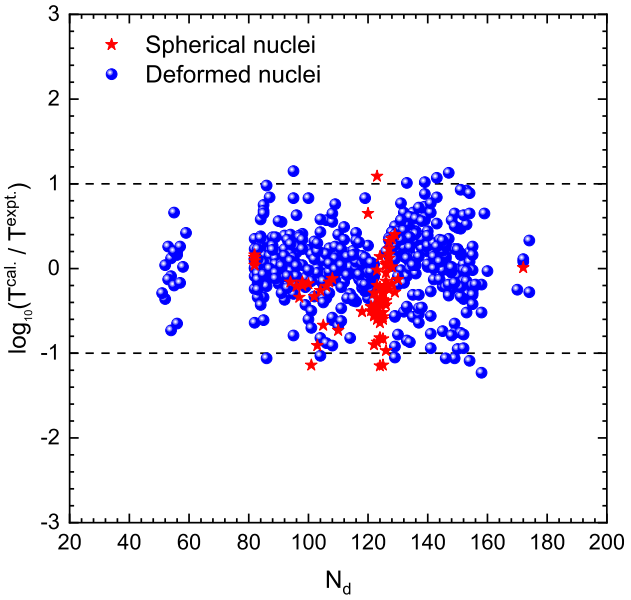

Fig. 2 Deviation of the calculated and experimental α-decay half-lives versus the neutron number, N_d, of daughter nuclei. Red star points denote the results for spherical or moderately deformed α emitters and blue circle points denote the results for well deformed α emitters

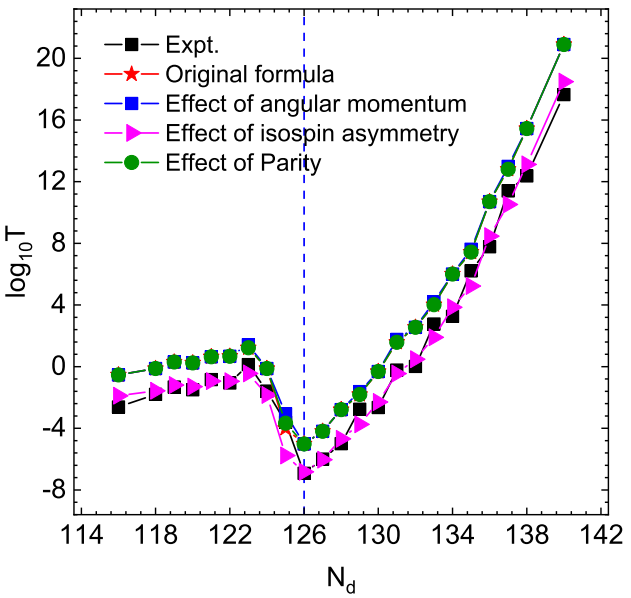

Fig. 3 Comparison of effects of angular momentum, isospin asymmetry and parity on the variation of $\log_{10} T$ against the number of neutrons of the daughter nuclei for different isotopes of Th ($Z = 90$). These terms represent decomposition of each contribution of Formula E, Eq. (6)

angular momentum and parity [68].

$$\ell_{min} = \begin{cases} \Delta_j, & \text{for even } \Delta_j \text{ and } \pi_p = \pi_d, \\ \Delta_j + 1, & \text{for even } \Delta_j \text{ and } \pi_p \neq \pi_d, \\ \Delta_j, & \text{for odd } \Delta_j \text{ and } \pi_p \neq \pi_d, \\ \Delta_j + 1, & \text{for odd } \Delta_j \text{ and } \pi_p = \pi_d, \end{cases} \quad (3)$$

Table 2 The parameters of proposed FB for all sets of α emitters

Set	a	b	c	d
e–e	0.402453	− 1.48927	− 12.2981	0
e–o	0.410496	− 1.44560	− 14.0945	0.043999
o–e	0.409667	− 1.45629	− 13.7325	0.017331
o–o	0.417194	− 1.40325	− 15.6988	0.037728
All nuclei	0.404460	− 1.44180	− 13.5091	0.039790

Table 3 The parameters of proposed FC for all sets of α emitters

Set	a	b	c	e	f
e–e	0.410918	− 1.4212	− 15.2909	10.7387	−56.9910
e–o	0.409963	− 1.3572	− 15.5186	−8.1508	25.7466
o–e	0.423354	− 1.3237	− 17.1794	−10.9384	4.1279
o–o	0.420968	− 1.3981	− 15.8829	−1.8728	3.7592
All	0.407609	− 1.3944	− 14.9706	3.8275	−22.8059

where $\Delta_j = |j_p - j_d|$ with j_p, π_p, j_d, π_d being the spin and parity of the parent and daughter nuclei, respectively. For different sets of α-decay, the values of parameters a, b, c, and d are get by fitting the experimental data in Table 2.

2.3 NRDX formula including isospin asymmetry effect (Formula-C)

We modified the NRDX formula by adding nuclear isospin asymmetry terms, I and I^2 , $I = \frac{(N-Z)}{A}$ for parent nuclei, which has been demonstrated to play an important role for the determination of half-lives. The new relation is given as

$$\log_{10} T_{1/2} = a\sqrt{\mu}\, Z_c\, Z_d\, Q_c^{-1/2} + b\sqrt{\mu}\,(Z_c\, Z_d)^{1/2} + c + e\, I + f\, I^2, \quad (4)$$

Parameters a, b, c, e, and f are given in Table 3.

2.4 NRDX formula including both ℓ-angular momentum and isospin asymmetry effect (Formula-D)

By taking into account angular momentum for α-decay and isospin effect. The new relation is given as

$$\log_{10} T_{1/2} = a\sqrt{\mu}\, Z_c\, Z_d\, Q_c^{-1/2} + b\sqrt{\mu}\,(Z_c\, Z_d)^{1/2} + c + d\,\ell(\ell+1) + e\, I + f\, I^2. \quad (5)$$

Parameters a , b , c , d , e *and* f are given in Table 4.

2.5 NRDX formula including both ℓ-angular momentum, isospin asymmetry and parity effects (Formula-E)

We have included the parity effect, which is suggested in [68], in the calculations that may help to explain half-lives.

Table 4 The coefficients of proposed formula D for all sets of α emitters

Set	a	b	c	d	e	f
e–e	0.410918	− 1.4212	− 15.2909	0	10.7387	−56.9910
e–o	0.415379	− 1.3989	− 15.2438	0.04551	−6.5849	12.6399
o–e	0.421783	− 1.3356	− 16.9160	0.01276	−10.0799	5.3700
o–o	0.421888	− 1.3629	− 17.1955	0.03994	2.0780	−17.7730
All	0.409881	− 1.3990	− 15.2059	0.04055	3.4239	−23.8579

Table 5 The coefficients of proposed formula E for all sets of α emitters

Set	a	b	c	d	e	f	g
e–e	0.410918	− 1.42120	− 15.2909	0	10.73868	−56.9910	0
e–o	0.410796	− 1.42969	− 14.2146	0.022595	−2.25920	−0.53224	0.502634
o–e	0.424757	− 1.31517	− 17.6008	0.020609	−12.09466	10.0859	−0.134478
o–o	0.421951	− 1.39998	− 16.3099	0.030543	0.96066	−12.2475	0.227788
All nuclei	0.408505	− 1.41695	− 14.6766	0.027154	4.13841	−24.9919	0.244732

Therefore, the new modified formula is given by

$$\log_{10} T_{1/2} = a\sqrt{\mu}\, Z_c\, Z_d\, Q_c^{-1/2} + b\sqrt{\mu}\,(Z_c\, Z_d)^{1/2} + c + d\,\ell(\ell+1) + e\,I + f\,I^2 + g\,(1-(-1)^{\ell}) \quad (6)$$

Parameters a , b , c , d , e , f *and* g are given in Table 5.

Now we describe the cluster radioactivity data with the formulae FA-FE. We determine the parameters through a least square fit to the available data of 22 emitters have definite experimental values extracted from NUBASE2020 [66] in Table 6.

The standard deviations for each formula between experimental cluster and α-decay half-lives and calculations for all sets, 22 Clusters, and for α+cluster formulas, are listed in Tables 7 and 8. Also, we predict the cluster half-lives of 79 cluster using the formula E of (α+cluster). The predictions are listed in Table 10.

3 Results and discussions

Table 9 compares the experimental data of $\log_{10} T_c$ for 22 cluster decays with our calculations using using the five formulas FA, FB, FC, FD and FE given by Eqs. (1), (2), (4), (5), and (6), respectively. Equation (1) is NRDX formula FA [65] with updated parameters, while FB is the same as FA but with angular momentum term. FC is the NRDX formula modified to include isospin asymmetry term which is important for clusters and heavy nuclei. FD is the same as FB but isospin term is added, while FE is NRDX formula including angular momentum, isospin, and parity effects. The parameters of the five equations are determined from least square fitting to the recent experimental data of 595 cluster and α decay processes. Table 9 shows good agreement between our theoretical calculations and the available experimental data. This is evident from Table 8 for the standard deviations of the decimal logarithmic values which are given by

$$\sigma = \left[\frac{1}{n-1}\sum_{k=1}^{n}\left(\log_{10} T_{1/2}^{\text{calc.}} - \log_{10} T_{1/2}^{\text{expt.}}\right)^2\right]^{1/2}, \quad (7)$$

where n denotes the number of nuclei and $\log_{10} T_{1/2}^{\text{calc.}}$ has the five values given by Eqs. (1), (2), (4), (5), and (6). Table 8 shows that the $\log T^{\text{cal}}$ given by Eq. (6) for cluster decays and denoted by FE has the lowest RMS values. The maximum difference between FE and the experimental value is 1.45 for ^{28}Mg emission from ^{236}Pu which represents percentage difference of 6.7%. Table 8 shows also that Formula E for α and cluster decays has the lowest RMS value. We compare our formulas with commonly used similar ones for cluster emission. In Table 8, we present the values of RMS of Horoi and NUDL for the 22 cluster decay shown in Table 9 and the 595 cluster and α emissions. The values of RMS show clearly that our formulas are better than the two others.

We considered 573 α-emitters and compared the values of $\log_{10} T_{1/2}^{\text{calc.}}$ with the corresponding latest experimental data for the four sets of nuclei: even Z − even N (e−e), even Z − odd N (e−o), odd Z − even N (o−e), and odd Z − odd N (o−o). The comparison is presented in Fig. 1, which depicts the variation of $\log_{10}\left(T_{1/2}^{\text{calc.}}/T_{1/2}^{\text{expt.}}\right)$ against the number of neutrons of the daughter nuclei, N_d. The computation of $\log_{10} T_{1/2}^{\text{calc.}}$ was performed using the five Eqs. (1), (2), (4), (5), and (6). Figure 1a shows good agreement between theoretical and experimental half-lives. Almost all of the points in the Fig. 1a are located between the two horizontal lines $\log_{10} T_{1/2}^{\text{calc.}}/T_{1/2}^{\text{expt.}} = \pm 1$. Moreover, most of the points of FD and FE lie on or around the line $\log_{10}\left(T_{1/2}^{\text{calc.}}/T_{1/2}^{\text{expt.}}\right) = 0$.

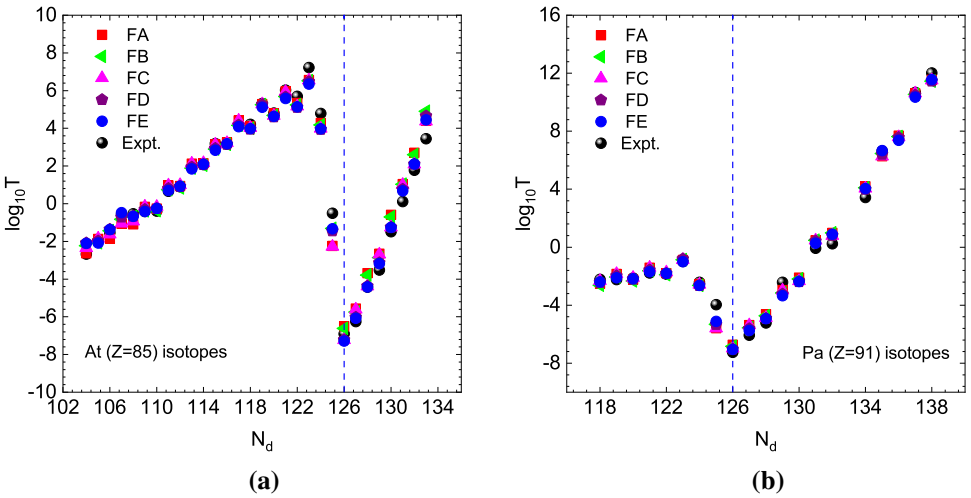

Fig. 4 Comparison of the logarithmic α-decay half-lives with the neutron number, N_d, of daughter nuclei for different isotopes of **a** At ($Z = 85$), **b** Pa ($Z = 91$) nuclei

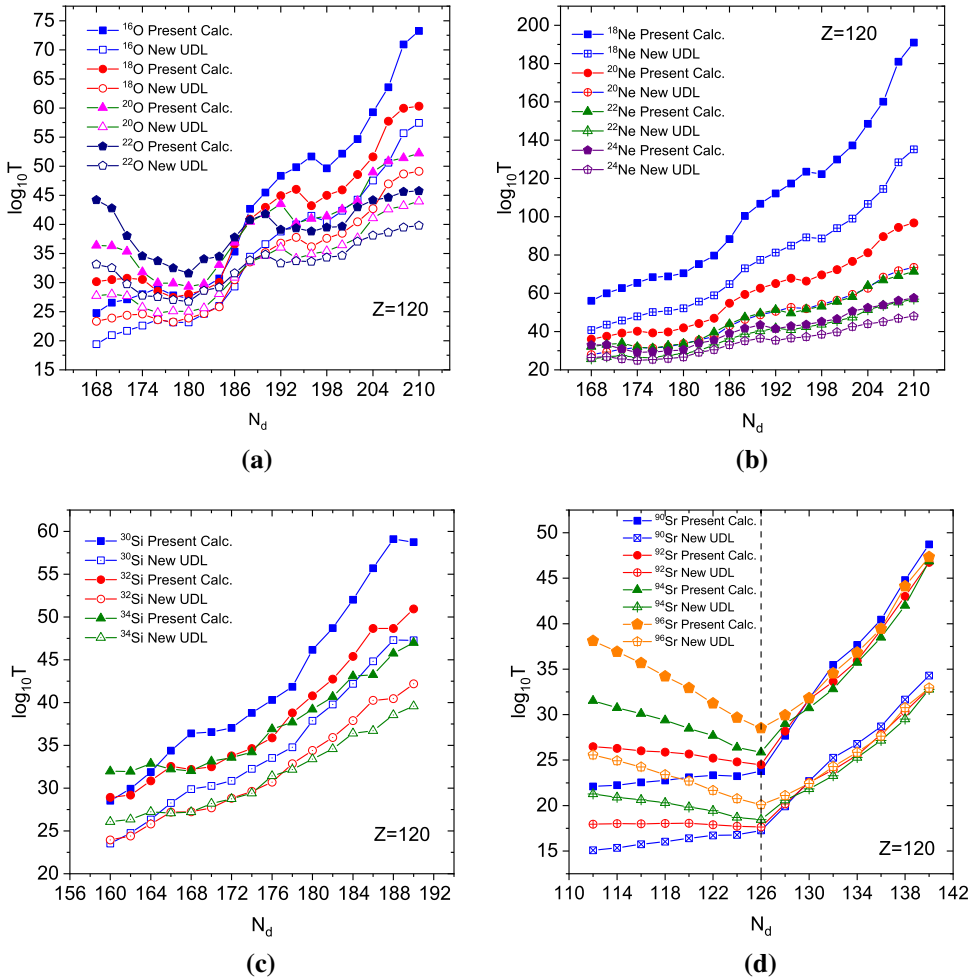

Fig. 5 The possible cluster emissions from the SHN with $Z = 120$ using the present calculation and compared with new UDL formula

Table 6 The coefficients of proposed formulas for cluster decay

Set	a	b	c	d	e	f	g
Formula A (cluster only)	0.359267	− 1.01087	−18.2003	0	0	0	0
Formula B (cluster only)	0.369203	− 1.03579	−19.86599	0.058336	0	0	0
Formula C (cluster only)	0.337327	− 0.94173	−97.74909	0	723.2921	−1606.5483	0
Formula D (cluster only)	0.338789	− 0.93866	62.63012	0.065217	−828.1781	2113.6610	0
Formula E (cluster only)	0.342684	− 0.95099	47.66104	0.061255	−682.2041	1751.8500	0.10534
Formula A (α+cluster)	0.405276	− 1.16300	−20.5934	0	0	0	0
Formula B (α+cluster)	0.406282	− 1.16590	−20.7782	0.035075	0	0	0
Formula C (α+cluster)	0.419082	− 1.20188	−19.9022	0	−8.44171	−6.56093	0
Formula D (α+cluster)	0.421158	− 1.20783	−20.0939	0.040684	−8.6552	−8.1492	0
Formula E (α+cluster)	0.421065	− 1.20758	−20.0631	0.031564	−8.99572	−7.82254	0.168524

Table 7 RMS of proposed formulae for all sets of α emitters

Formula	e–e	e–o	o–e	o–o	All nuclei
FA	0.3909	0.6144	0.5296	0.6277	0.6343
FB	0.3909	0.5313	0.4995	0.5017	0.5511
FC	0.3207	0.6105	0.4750	0.6275	0.6269
FD	0.3207	0.5246	0.4580	0.4917	0.5394
FE	0.3207	0.4471	0.4506	0.4565	0.5211

Figs. 1b–d are the same as Fig. 1a but for e−o, o−e and o−o, respectively. For the calculated values using FA, FB, and FC, the majority of the points are located above or below the two horizontal lines $\log_{10} T_{1/2}^{\text{calc.}}/T_{1/2}^{\text{expt.}} = \pm 1$. The points representing FD and FE are located at or near the middle line $T_{1/2}^{\text{expt.}} = T_{1/2}^{\text{calc.}}$. In general, Fig. 1 shows a satisfactory agreement between the five formulas for α-emission and the recent experimental data. Since most of the nuclei considered in the present work are deformed, it is interesting to demonstrate the accuracy of our formula in case of deformed nuclei. We consider 498 well-deformed α emitters and 75 spherical or moderately deformed ones. The quadrupole deformation parameter of the studied nuclei ranges between 0.05 and 0.33, while the hexadecapole deformation parameter has a maximum value of 0.127 [69]. The deviations of calculated α-decay half-lives from the experimental data are plotted as a function of the neutron number of daughter nuclei, N_d, in Fig. 2. Red star points denote the results for spherical or moderately deformed α emitters and blue circle points denote the results for well deformed α emitters. The standard deviations of the decimal logarithmic values given by Eq. (7) for spherical or moderately deformed α emitters is 0.7455, while for well deformed α emitters is 0.5558. The small value of σ for deformed nuclei relative to spherical ones may be a result of the large number of deformed nuclei, which is approximately 6.6 times greater than the number of spherical nuclei.

Figure 3 depicts a comparison of the effects of angular momentum, isospin asymmetry and parity on the variation of $\log_{10} T$ versus the number of neutrons of the daughter nuclei for various isotopes of Th ($Z = 90$). These terms represent decomposition of each contribution of Formula E, Eq. (6). Figure 3 shows that the effect of angular momentum on $\log_{10} T$ variation is the same as the parity effect, while the isospin asymmetry effect almost coincides on the experimental data. The original formula curve with the coefficients a, b, and c is above the experimental one. This demonstrates the importance of isospin asymmetry correction for heavy nuclei.

Despite their simplicity, the proposed formulas produce the α-decay half-lives for a large number of nuclei with nearly the same accuracy as microscopic calculations, which require much computational time and cannot be applied to a large number of nuclei. The ability of the simple analytical formulas to generate the characteristic features of the $\log_{10} T$ variation curve against the neutron number of daughter nuclei of various isotopes of a specific element is another test of their validity. In order to perform this test, the isotopes of two heavy elements with Z values of 85 and 91 are considered. Figure 4a, b present the variation of $\log_{10} T$ versus N_d for the α-emitter parent nuclei with $Z_p = 85$ and 91, respectively. The curve of $\log_{10} T$ for each element passes through a minimum value at the neutron magic number $N_d = 126$. After the minimum (when $N_d > 126$), each curve increases linearly as N_d increases. The minimum is due to the existence of two neutrons that can be easily extracted from the neutron level $9/2^+$, which has a capacity of 10 neutrons.

At $N_d = 126$, $\log_{10} T$ inverts its behavior and begins to increase with decreasing N_d, until it reaches its maximum value at $N_d = 123$. At this maximum, the cluster (α-particle) takes its two neutrons from levels below the gap. As N_d decreases, the cluster still gets its neutrons from below the gap, while at the right of the maximum cluster builds its two neutrons from the upper gap levels and from levels above the

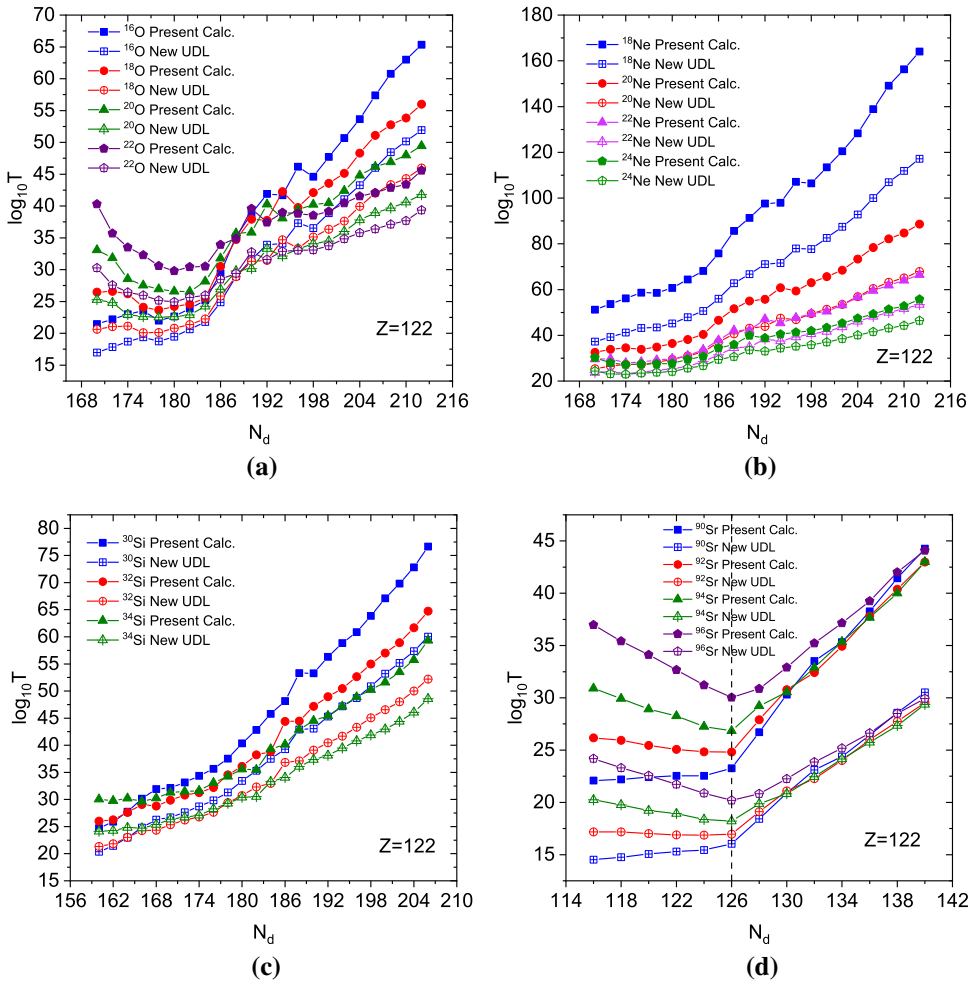

Fig. 6 The same as Fig. 5 but for the SHN with $Z = 122$

gap. The $\log_{10} T$ curve decreases linearly as N_d decreases. The maximum at $N_d = 125-$number of neutrons in the cluster for α-emission, $N_d = 123$, characterizes all cluster emission curves at least for the magic number $N = 126$ [70].

We test the simple formula given by Eq. (6) for cluster emission from the superheavy nuclei with $Z = 120$, 122, 124, and 126. We compare the results of $\log_{10} T_c$ calculated from Eq. (6) to the corresponding results obtained from the New UDL (NUDL) formula given in Ref. [50]. We consider isotopes of four clusters, namely, O, Ne, Si, and Sr. It should be noted that NUDL formula for α- and cluster emission is one of the successful formulas in producing the experimental data [66]. Figure 5 shows the N_d variation of $\log_{10} T_c$ for emission of four O isotopes, four Ne isotopes, three Si isotopes, and four Sr isotopes from the superheavy nucleus with $Z = 120$. Figure 5a is for the emission of ^{16}O, ^{18}O, ^{20}O, and ^{22}O from the parent nucleus with $Z = 120$, leaving the daughter nucleus with $Z = 112$. The $\log_{10} T$ curves in Fig.5a show a clear minimum at $N_d = 180$. The behavior of $\log_{10} T_c$ for NUDL is almost the same as that of our formula for all O-clusters isotopes; the difference between the two formulas is the magnitude of $\log_{10} T_c$. Beside the minimum at $N_d = 180$, there are two other minima at $N_d = 196$ for ^{18}O and $N_d = 198$ for ^{16}O. These minima have depths that are too shallow and do not exist for other isotopes. Thus, the three above mentioned minima can be produced by arranging the neutron levels for $Z = 112$ as shown in neutron schemes of Fig. 9a, b. Figure 5b is the same as Fig. 5a but for the isotopes of Ne cluster, the daughter nucleus is the superheavy nucleus with $Z = 110$. Figure 5b shows two minima with

Table 8 RMS of proposed formulae for cluster decay

Formula	F–A	F–B	F–C	F–D	F–E	Horoi	NUDL
Cluster only	0.6493	0.5746	0.6262	0.5410	0.5355	0.8651	0.7481
α+cluster	0.8151	0.7671	0.6767	0.597	0.5888	0.9127	6.1988

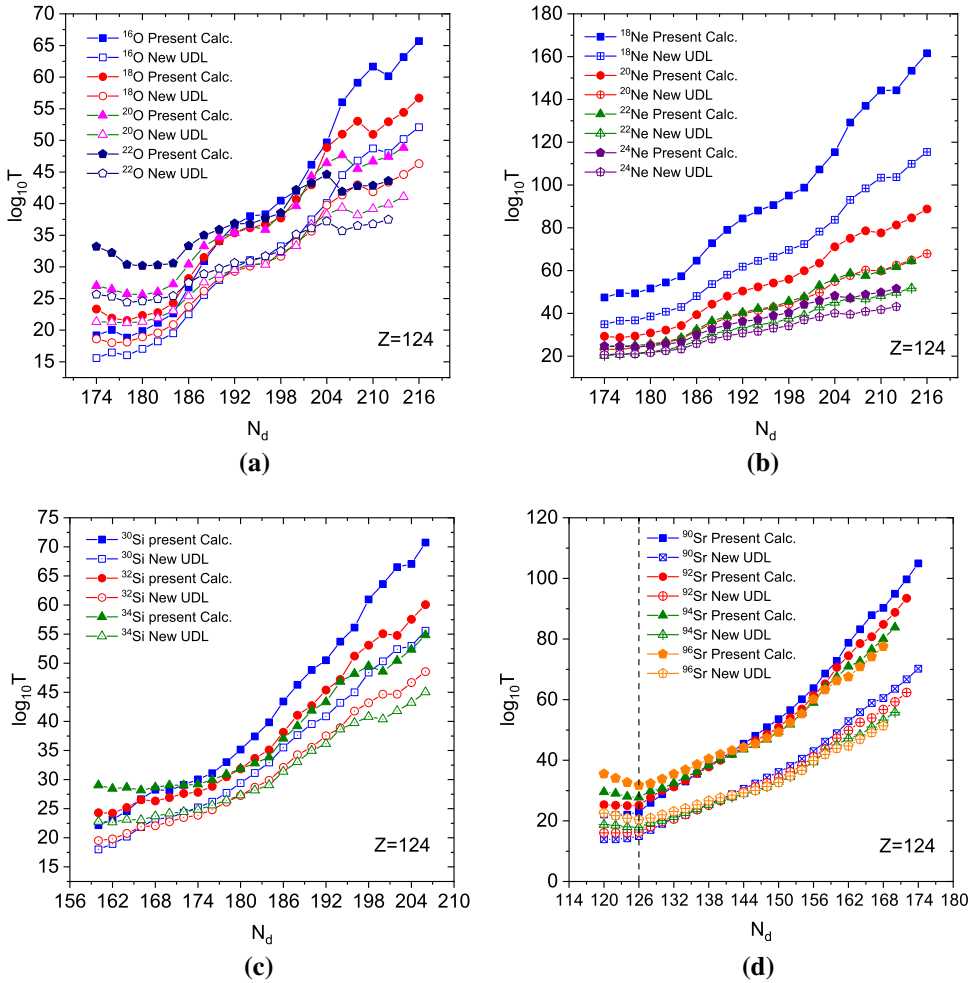

Fig. 7 The same as Fig. 5 but for the SHN with $Z = 124$

small depths for ^{20}Ne and ^{18}Ne, respectively, at $N_d = 196$ and 198. There are no other minima found for the other Ne isotopes. The neutron level scheme of Fig. 9b shows the level closure at $N_d = 196$, while the level arrangement needs to be changed to produce neutron level closure at $N_d = 198$. This can be done by moving $j_{13/2}$ level downwards to follow $2h_{11/2}$ level as shown in scheme of Fig. 9b. Another method to get the neutron stability at 198 is to change the levels strongly as seen in scheme of Fig. 9c. This Scheme agrees with the calculations of Ref. [71] for $Z = 126$ superheavy nucleus. Figure 5c is the same as Fig. 5a but for different Si cluster isotopes while the daughter nucleus is Sg with $Z = 106$. Figure 5c does not show minima for any of the three isotopes of Si element. Figure 5d is for the Sr cluster emissions from $Z = 120$ superheavy nucleus, the daughter nucleus is the heavy element Pb. The minimum in Fig. 5d is the well-known magic neutron number $N_d = 126$. This minimum is clear for the isotopes ^{96}Sr and ^{94}Sr but not clear for ^{92}Sr and vanishes for the cluster ^{90}Sr. For $N_d = 126$, the parent nucleus is ^{298}120 for ^{90}Sr emission and ^{304}120 for ^{96}Sr decay. The number of neutrons in ^{298}120 is 178, while the number in ^{304}120 is 184. These two neutron numbers correspond to neutron level closures [71]. The self-consistent mean-field calculations in [72] provided evidences on possible magicity at these two neutron numbers 178 and 184, which are consistent with the results in [10,11]. For N_d variation in the range $112 \leq N_d \leq 126$, the number of neutrons in the parent nucleus varies from $N_p = 164$ to 178 for ^{90}Sr emission and from 170 to 184 for ^{96}Sr cluster emission. According to neutron level scheme of Fig. 9d, the cluster ^{90}Sr builds its neutrons from $3d_{5/2}$ and the levels below it. ^{96}Sr, on the other hand, gets its neutrons from $4s_{1/2}$ and the levels below it. In the range $128 \leq N_d \leq 140$, the neutron number of the parent nucleus N_p varies from 180 to 192 for ^{90}Sr and from 186 to 198 for ^{96}Sr. In this variation range, the ^{90}Sr cluster builds its neutrons from the level above $4s_{1/2}$ and levels below it, whereas the ^{96}Sr cluster gets its neutrons from $j_{13/2}$ level and below it. The number of protons in Sr is 38, and the proton scheme in Fig. 9e shows that the cluster gets their protons from the levels depicted in this scheme. The 38 protons are taken from $1h_{9/2}$ level and levels above till $2f_{5/2}$ proton level. Note that the proton levels are completely filled.

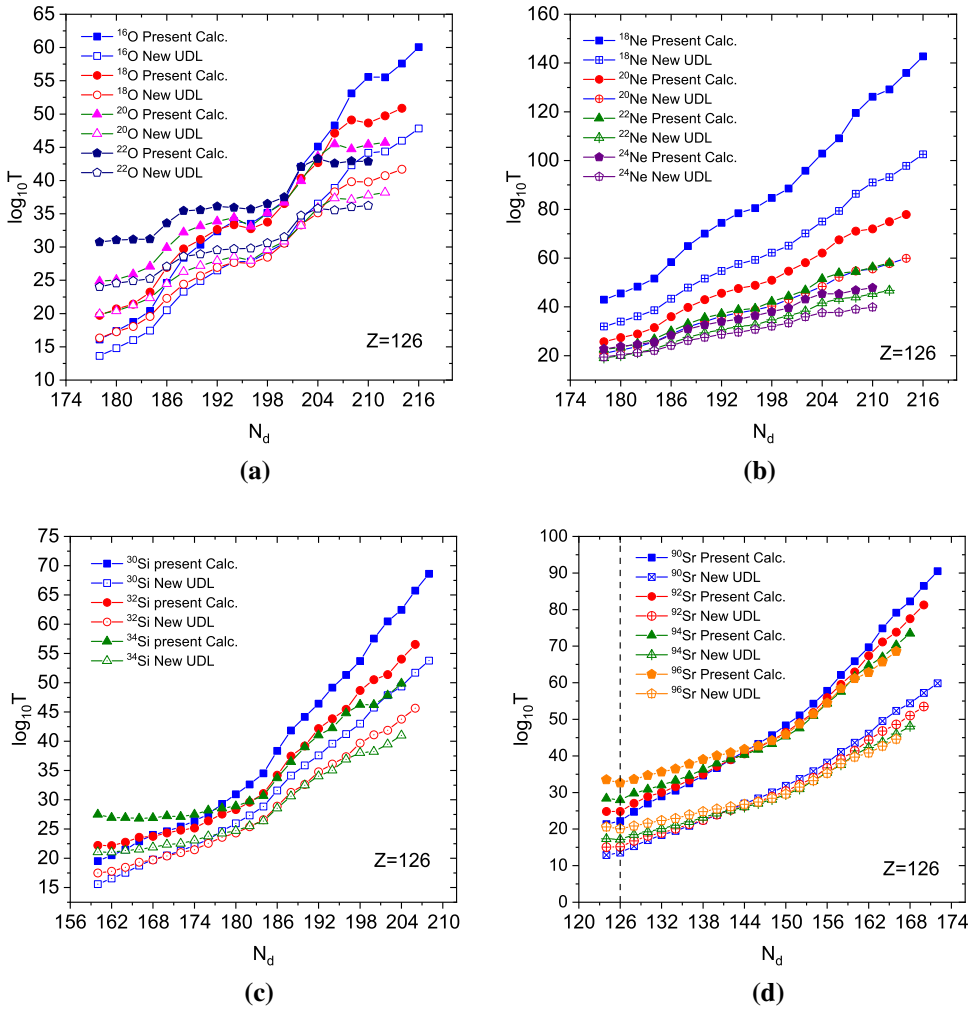

Fig. 8 The same as Fig. 5 but for the SHN with $Z = 126$

The scheme proposed two proton magic numbers, 114 and 120. The protons extracted from the Sr cluster are all above the proton magic number $Z = 82$. This may be the reason of the linear dependence of $\log_{10} T$ as N_d varies.

Figure 6 is the same as Fig. 5 but for the cluster decay of the parent superheavy nucleus $Z = 122$. Figure 6a shows isotopes of O emission from $Z = 122$ leaving the daughter nucleus with $Z = 114$. Variation of $\log T_c$ for different isotopes of O nucleus against N_d shows two clear minima at $N_d = 178$ for ^{16}O and ^{18}O, and $N_d = 180$ for ^{20}O and ^{22}O. Two other minima with small depths are shown at $N_d = 196$ for ^{18}O and $N_d = 198$ for ^{16}O. Neutron level schemes of Fig. 9a, b show that these four neutron number correspond to the following levels, $4s_{1/2}$ for $N_d = 180$, $3d_{5/2}$ for 178, $4s_{1/2}$ for 196, and $j_{13/2}$ for $N_d = 198$.

Figure 6b is the same as Fig. 6a except it is for the emission of Ne isotopes, where the daughter nuclei are the isotopes of copernicium with $Z = 112$. Figure 6b shows three minima: $N_d = 194$ for ^{22}Ne, $N_d = 196$ for ^{20}Ne, and $N_d = 198$ for ^{18}Ne. These three neutron numbers could be explained from the neutron level arrangements in scheme of Fig. 9b. In Fig. 6c, there are no obvious minima for the three Si isotopes. The daughter nucleus in this case is hassium ($Z = 108$). Figure 6d is for the Sr cluster emissions from $Z = 122$ superheavy nucleus, where the daughter nucleus is the heavy element Po. Figure 6d shows nearly the same log T_c variation with N_d as shown in Fig. 5d for $Z = 120$.

Figure 7 is the same as Fig. 5, except that it depicts cluster emissions from the parent superheavy nucleus with $Z = 124$. Figure 7a–d are for O, Ne, Si, and Sr isotopes, respectively, leaving daughter nuclei with $Z = 116$, 114, 110 and 86. Figure 7a shows a minimum at $N_d = 178$ for ^{16}O and ^{18}O, as well as three other minima at $N_d = 206$ for ^{22}O, $N_d = 210$ for ^{18}O, and $N_d = 212$ for ^{16}O. The neutron number 178 corresponds to $3d_{5/2}$ level as shown in the scheme of Fig. 9a. The other three neutron numbers 206, 210, and 212 could be explained from the neutron level arrangements in schemes of Fig. 9f, g. For the emission of Ne isotopes, Fig. 7b shows two minima: $N_d = 210$ for ^{20}Ne and $N_d = 212$ for ^{18}Ne. Two shallow minima were observed for the emission of Si isotopes at $N_d = 200$ for ^{34}Si and $N_d = 202$ for ^{32}Si in Fig. 7c. These neutron numbers could be explained from the neutron

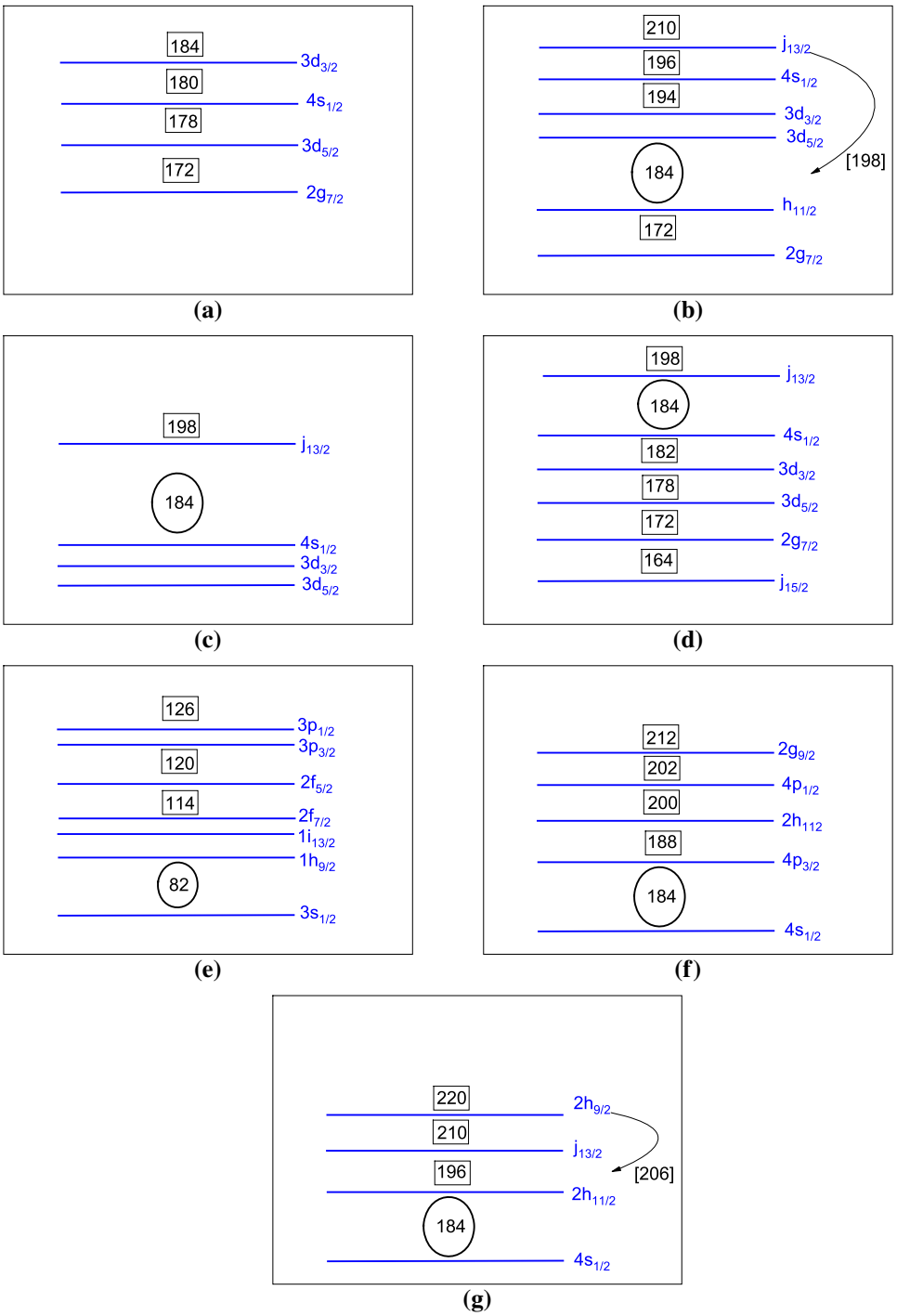

Fig. 9 The neutron level schemes **a**–**d**, **f**, and **g**, while **e** is for proton level scheme

level arrangements in scheme of Fig. 9f. For the emission of Sr isotopes, as shown in Fig. 7d, $\log_{10} T$ curves have the minimum at $N_d = 126$, as expected but this minimum is not clear for all isotopes.

Figure 8 depicts cluster emissions of O, Ne, Si, and Sr isotopes from the superheavy nucleus with $Z = 126$. For emission of O isotopes, Fig. 8a shows minima at $N_d = 196$ for ^{20}O, $N_d = 206$ for ^{22}O and $N_d = 210$ for ^{18}O. These neutron numbers could be explained by the neutron level arrangements depicted in the scheme of Fig. 9. There are no observed minima in Fig. 8b–d. It is worth mentioning that in α- or cluster decays, the half-life time becomes minimum when the neutron and/or proton numbers of the corresponding residual daughter nucleus are magic [73,74]. This indicates that the parent nucleus decays to a more stable configuration in the daughter nucleus. The depth of this mini-

Table 9 Calculations of cluster-decay half-lives. The experimental cluster decay half-lives, spin and parity are taken from the latest evaluated nuclear properties table NUBASE2020 [66],“ *” means directly measured spin. The cluster-decay energy is taken from the latest evaluated atomic mass table AME2020 [67]. The cluster-decay energy is in the unit of MeV

Parent	Daughter	Cluster	$Q_C^{\text{Expt.}}$(MeV)	J_p^π	J_d^π	$\ell_{\min}$	$\log_{10} T_c$					
							Expt.	FA	FB	FC	FD	FE
^{221}Fr	^{207}Tl	^{14}C	31.292	$5/2^-*$	$1/2^+*$	3	14.52	14.07	14.39	13.91	14.26	14.46
^{221}Ra	^{207}Pb	^{14}C	32.396	$5/2^+*$	$1/2^-*$	3	13.32	12.85	13.17	12.75	13.11	13.30
^{222}Ra	^{208}Pb	^{14}C	33.049	0^+	0^+	0	11.05	11.60	11.49	11.41	11.28	11.24
^{223}Ra	^{209}Pb	^{14}C	31.828	$3/2^+*$	$9/2^+$	4	15.05	13.99	14.59	13.85	14.53	14.31
^{224}Ra	^{210}Pb	^{14}C	30.535	0^+	0^+	0	15.90	16.68	16.58	16.59	16.47	16.43
^{226}Ra	^{212}Pb	^{14}C	28.197	0^+	0^+	0	21.29	22.00	21.92	22.01	21.92	21.88
^{225}Ac	^{211}Bi	^{14}C	30.477	$3/2^-$	$9/2^-*$	4	17.21	17.84	18.45	17.85	18.55	18.33
^{228}Th	^{208}Pb	^{20}O	44.723	0^+	0^+	0	20.73	21.98	21.90	22.14	22.05	22.01
^{230}U	^{208}Pb	^{22}Ne	61.388	0^+	0^+	0	19.56	20.05	19.96	20.27	20.18	20.15
^{230}Th	^{206}Hg	^{24}Ne	57.760	0^+	0^+	0	24.61	24.69	24.61	24.87	24.79	24.75
^{231}Pa	^{207}Tl	^{24}Ne	60.410	$3/2^-*$	$1/2^+*$	1	22.89	21.78	21.76	21.92	21.91	22.19
^{232}U	^{208}Pb	^{24}Ne	62.310	0^+	0^+	0	20.39	20.21	20.13	20.37	20.27	20.23
^{233}U	^{209}Pb	^{24}Ne	60.486	$5/2^+*$	$9/2^+$	2	24.84	23.15	23.28	23.36	23.52	23.43
^{234}U	^{210}Pb	^{24}Ne	58.825	0^+	0^+	0	25.93	25.94	25.87	26.21	26.14	26.10
^{234}U	^{208}Pb	^{26}Ne	59.413	0^+	0^+	0	25.93	26.57	26.50	26.87	26.80	26.76
^{234}U	^{206}Hg	^{28}Mg	74.110	0^+	0^+	0	25.74	24.89	24.81	25.14	25.06	25.02
^{235}U	^{207}Hg	^{28}Mg	72.425	$7/2^-*$	$9/2^+$	1	27.44	27.49	27.50	27.80	27.81	28.09
^{236}Pu	^{208}Pb	^{28}Mg	79.669	0^+	0^+	0	21.65	20.13	20.04	20.33	20.24	20.20
^{238}Pu	^{210}Pb	^{28}Mg	75.911	0^+	0^+	0	25.66	25.58	25.51	25.90	25.83	25.79
^{238}Pu	^{208}Pb	^{30}Mg	76.796	0^+	0^+	0	25.66	25.62	25.55	25.94	25.87	25.83
^{238}Pu	^{206}Hg	^{32}Si	91.187	0^+	0^+	0	25.30	24.73	24.66	25.03	24.96	24.92
^{242}Cm	^{208}Pb	^{34}Si	96.510	0^+	0^+	0	23.11	22.41	22.33	22.67	22.59	22.55

mum is dependent on the degree of stability of the daughter nucleus, with a deeper minimum corresponding to a more stable nucleus [73]. The investigation of microscopic shell and pairing correction energies [10,11,75] provided evidences on possible magicity and enhanced stability at neutron numbers $N = 178$, 180, 184, 190, 206, 210, and 212 predicted in the present work.

4 Summary and conclusion

Improved empirical NRDX formulas for α- and cluster emission half-lives are presented by considering the effects of centrifugal potential, isospin asymmetry and parity. The coefficients of the modified formulas are fitted using the latest experimental half-lives for 573 α-emitters in the Z-range $52 \leq Z \leq 118$ and 22 experimental cluster decays. The modified formulas were used to study α-decay half-lives from the isotopes of two heavy elements. The formulas produce the experimental α-decay half-lives with good accuracy and succeeded in predicting the variation of $\log_{10} T$ with neutron numbers of the daughter nuclei for the two heavy elements.

The good agreement between our improved formula and α-decay half-lives beside the simplicity of the calculations encouraging to extend the simple formula to calculate the half-lives of cluster emission from several nuclei. We found that our results for cluster emission agree well with other known formulas. We applied the present formula of cluster half-lives to emission of four O, four Ne, three Si, and four Sr isotopes from the SHN with $Z = 120$, 122, 124, and 126. We compared our results with NUDL formula. Based on the neutron number values correspond to dips or minima, we tried to predict the neutron energy levels of four SHN with $Z = 120$, 122, 124, and 126. These SHN are not yet experimentally synthesized.

Table 10 Predicted $\log_{10} T_{1/2}$ values for nuclei emitting heavier clusters by Formula E (α+cluster) and the results of UDL [61](α+cluster), new UDL(NUDL) [50], MGLDM [31] as well as Bao et al. [32] are in the unit s. Q_c values are in terms of MeV and they are taken from Ref. [31]. The spin and parity of nuclei are taken from the latest evaluated nuclear properties c [66] where "()" means uncertain spin and/or parity, "*" means directly measured spin and "#" means values estimated from trends in neighboring nuclei

Parent	Daughter	Cluster	Q_C	J_p^π	J_d^π	$\ell_{\min}$	$\log_{10} T_c$					
							Present calc.	Horoi	UDL [61]	NUDL [50]	MGLDM [31]	Bao [32]
^{220}Ra	^{208}Pb	^{12}C	32.13	0^+	0^+	0	10.71	10.02	12.61	10.98	12.14	11.75
^{222}Ra	^{204}Hg	^{18}O	39.94	0^+	0^+	0	26.91	25.65	28.06	23.71	27.20	28.08
^{226}Ra	^{206}Hg	^{20}O	40.96	0^+	0^+	0	26.91	26.26	27.73	24.74	25.72	26.57
^{224}TH	^{200}Hg	^{24}Ne	55.63	0^+	0^+	0	28.82	27.62	29.43	25.35	27.84	29.49
^{226}TH	^{202}Hg	^{24}Ne	56.68	0^+	0^+	0	26.82	25.92	27.47	24.49	26.52	26.90
^{228}TH	^{204}Hg	^{24}Ne	57.59	0^+	0^+	0	25.11	24.48	25.80	23.83	25.72	25.43
^{230}U	^{210}Po	^{20}O	43.93	0^+	0^+	0	26.49	25.40	26.96	22.86	25.37	26.18
^{230}U	^{206}Pb	^{24}Ne	61.54	0^+	0^+	0	21.56	21.21	22.25	20.70	23.28	21.97
^{230}U	^{198}Os	^{32}S	85.85	0^+	0^+	0	46.85	43.36	45.44	27.05	29.90	29.89
^{232}U	^{204}Hg	^{28}Mg	74.54	0^+	0^+	0	24.40	24.50	24.52	23.86	25.10	24.90
^{236}Pu	^{212}Po	^{24}Ne	59.42	0^+	0^+	0	28.33	27.17	28.23	25.22	28.31	28.57
^{238}Cm	^{206}Pb	^{32}Si	97.58	0^+	0^+	0	20.11	22.11	19.33	20.56	23.34	21.43
^{240}Cm	^{210}Po	^{30}Mg	76.81	0^+	0^+	0	29.52	29.15	28.21	26.46	26.40	29.08
^{240}Cm	^{206}Pb	^{34}Si	95.74	0^+	0^+	0	23.67	25.38	22.11	23.26	25.21	24.28
^{242}Cm	^{210}Pb	^{32}Si	93.89	0^+	0^+	0	25.02	26.19	23.67	24.58	25.96	25.11
^{220}Ra	^{204}Hg	^{16}O	39.84	0^+	0^+	0	24.60	22.90	26.13	21.56	24.98	27.58
^{224}Ra	^{204}Hg	^{20}O	39.86	0^+	0^+	0	29.44	28.57	30.15	25.94	28.56	29.40
^{224}Th	^{210}Po	^{14}C	33.05	0^+	0^+	0	13.39	12.87	14.85	12.63	13.64	13.26
^{224}Th	^{208}Pb	^{16}O	46.63	0^+	0^+	0	14.57	13.70	16.52	14.66	19.38	15.81
^{226}Th	^{212}Po	^{14}C	30.66	0^+	0^+	0	18.43	17.87	19.56	16.44	17.72	18.30
^{226}Th	^{208}Pb	^{18}O	45.88	0^+	0^+	0	17.87	17.17	19.36	17.45	17.85	18.18
^{228}Th	^{214}Po	^{14}C	28.33	0^+	0^+	0	23.95	23.33	24.73	20.54	22.31	24.04
^{230}U	^{216}Rn	^{14}C	28.46	0^+	0^+	0	26.04	25.05	26.52	21.11	24.04	26.04
^{230}U	^{202}Hg	^{28}Mg	74.2	0^+	0^+	0	24.99	24.92	25.17	23.82	26.85	25.15
^{232}U	^{200}Pt	^{32}Si	85.54	0^+	0^+	0	29.27	29.44	28.59	27.74	29.63	29.58
^{234}Pu	^{210}Po	^{24}Ne	62.45	0^+	0^+	0	23.15	22.57	23.45	21.39	24.45	23.46
^{234}Pu	^{206}Pb	^{28}Mg	79.39	0^+	0^+	0	20.67	21.31	20.77	20.62	22.60	21.73

Table 10 continued

Parent	Daughter	Cluster	Q_C	J_p^π	J_d^π	$\ell_{\min}$	$\log_{10} T_c$					
							Present calc.	Horoi	UDL [61]	NUDL [50]	MGLDM [31]	Bao [32]
^{234}Pu	^{202}Hg	^{32}Si	92.04	0^+	0^+	0	23.82	25.00	23.21	23.38	26.25	24.26
^{236}Pu	^{204}Hg	^{32}Si	91.93	0^+	0^+	0	23.92	25.15	23.18	23.85	25.98	24.68
^{238}Cm	^{210}Po	^{28}Mg	80.66	0^+	0^+	0	22.24	22.66	21.89	21.29	23.99	22.79
^{240}Cm	^{208}Pb	^{32}Si	97.82	0^+	0^+	0	19.74	21.88	18.85	20.73	22.67	20.26
^{242}Cm	^{208}Pb	^{34}Si	96.79	0^+	0^+	0	22.17	24.24	20.57	22.66	23.98	21.91
^{242}Cf	^{210}Po	^{32}Si	99.7	0^+	0^+	0	21.05	22.97	19.80	20.81	24.32	21.53
^{242}Cf	^{208}Po	^{34}Si	97.1	0^+	0^+	0	25.73	27.05	23.75	23.83	26.74	25.15
^{244}Cf	^{210}Po	^{34}Si	97.67	0^+	0^+	0	24.89	26.45	22.83	23.67	25.98	24.46
^{246}Cf	^{208}Pb	^{38}S	113.02	0^+	0^+	0	24.40	27.43	21.42	24.21	23.32	23.20
^{244}Cm	^{210}Pb	^{34}Si	93.42	0^+	0^+	0	26.87	28.11	24.84	26.12	27.23	26.18
^{242}Cf	^{206}Pb	^{36}S	114.16	0^+	0^+	0	22.03	25.10	19.97	21.97	25.25	22.92
^{223}Ra	^{205}Hg	^{18}O	40.45	$3/2^+*$	$1/2^-*$	1	26.18	24.65	26.97	23.20	24.17	26.83
^{225}Ac	^{207}Tl	^{18}O	43.6	$3/2^-$	$1/2^+*$	1	21.18	19.94	22.17	19.76	20.13	21.11
^{229}Th	^{205}Hg	^{24}Ne	58.01	$5/2^+*$	$1/2^-*$	3	25.05	23.83	25.03	23.54	25.30	24.86
^{225}Np	^{213}Fr	^{12}C	35.26	$9/2^-\#$	$9/2^-*$	0	9.91	8.81	11.50	8.39	11.55	10.38
^{225}Np	^{209}At	^{16}O	49.37	$9/2^-\#$	$9/2^-*$	0	13.84	12.77	15.63	12.45	16.23	14.72
^{227}Np	^{211}At	^{16}O	49.11	$5/2^+\#$	$9/2^-*$	3	14.90	13.15	15.91	13.19	16.01	15.28
^{227}Np	^{209}At	^{18}O	46.39	$5/2^+\#$	$9/2^-*$	3	21.72	19.69	22.07	17.79	20.14	21.00
^{231}Np	^{211}At	^{20}O	43.64	$5/2^+\#$	$9/2^-*$	3	29.26	27.19	28.80	23.81	27.03	28.23
^{233}Np	^{211}Bi	^{22}Ne	58.03	$5/2^+\#$	$9/2^-*$	3	28.01	25.84	27.77	24.46	27.67	27.97
^{237}Np	^{205}Au	^{32}Si	88.12	$5/2^+*$	$3/2^+\#$	2	27.55	28.02	26.41	26.89	28.55	28.26
^{237}Pu	^{205}Hg	^{32}Si	91.73	$7/2^-$	$1/2^-*$	4	24.81	25.40	23.36	24.22	25.89	25.00
^{237}Am	^{209}Bi	^{28}Mg	80.09	$5/2^-$	$9/2^-*$	2	21.52	21.92	21.17	21.08	22.76	21.89
^{237}Am	^{205}Tl	^{32}Si	94.74	$5/2^-$	$1/2^+*$	3	22.71	23.60	21.23	22.19	24.56	23.00
^{239}Am	^{207}Tl	^{32}Si	94.78	$5/2^-$	$1/2^+*$	3	22.60	23.59	21.00	22.52	24.59	23.11
^{239}Am	^{205}Tl	^{34}Si	93.44	$5/2^-$	$1/2^+*$	3	25.63	26.38	23.42	24.47	26.08	25.28
^{241}Am	^{207}Tl	^{34}Si	94.2	$5/2^-*$	$1/2^+*$	3	24.50	25.54	22.23	24.11	25.12	24.41
^{229}Th	^{215}Po	^{14}C	27.22	$5/2^+*$	$9/2^+$	2	27.03	26.18	27.42	22.67	24.75	27.04

Table 10 continued

Parent	Daughter	Cluster	Q_C	J_p^π	J_d^π	$\ell_{\min}$	$\log_{10} T_c$					
							Present calc.	Horoi	UDL [61]	NUDL [50]	MGLDM [31]	Bao [32]
^{231}Pa	^{209}Bi	^{22}O	42.56	$3/2^-*$	$9/2^-*$	4	30.68	29.32	30.07	26.12	27.13	29.40
^{231}Pa	^{203}Ir	^{28}Si	71.81	$3/2^-*$	$3/2^+$#	1	47.11	42.76	45.86	25.89	27.83	27.41
^{233}U	^{205}Hg	^{28}Mg	74.45	$5/2^+*$	$1/2^-*$	3	25.23	24.63	24.57	24.14	25.32	25.18
^{225}Np	^{211}Fr	^{14}C	32.83	$9/2^-$#	$9/2^-*$	0	17.17	16.13	18.18	13.35	16.52	16.49
^{227}Np	^{213}Fr	^{14}C	33.22	$5/2^+$#	$9/2^-*$	3	16.99	15.35	17.33	13.30	15.97	16.08
^{229}Np	^{211}At	^{18}O	46.37	$5/2^+$#	$9/2^-*$	3	21.68	19.74	22.00	18.27	20.31	21.26
^{231}Np	^{209}Bi	^{22}Ne	62.1	$5/2^+$#	$9/2^-*$	3	21.25	19.91	21.50	19.58	22.31	21.11
^{233}Np	^{209}Bi	^{24}Ne	62.36	$5/2^+$#	$9/2^-*$	3	22.44	21.38	22.22	20.85	23.64	22.04
^{235}Np	^{207}Tl	^{28}Mg	77.33	$5/2^+$	$1/2^+*$	2	22.08	22.42	21.93	22.23	23.61	23.00
^{237}Pu	^{207}Tl	^{30}Al	82.25	$7/2^-$	$1/2^+*$	3	28.13	27.51	26.68	26.02	28.20	28.23
^{239}Am	^{209}Bi	^{30}Mg	76.78	$5/2^-$	$9/2^-*$	2	27.90	27.67	26.65	25.66	27.31	27.32
^{239}Cm	^{207}Pb	^{32}Si	97.95	$7/2^-$#	$1/2^-*$	4	20.22	21.73	18.78	20.43	22.55	21.15
^{241}Cm	^{209}Pb	^{32}Si	95.67	$1/2^+$	$9/2^+$	4	23.22	24.20	21.46	22.79	24.45	22.86
^{243}Cm	^{209}Pb	^{34}Si	95.03	$5/2^+*$	$9/2^+$	2	24.78	26.23	22.77	24.44	26.01	24.08
^{249}Cf	^{203}Hg	^{46}Ar	125.08	$9/2^-$	$5/2^-*$	2	29.24	33.11	23.65	27.92	27.23	26.83
^{249}Cf	^{199}Pt	^{50}Ca	137.09	$9/2^-$	$5/2^-*$	2	30.99	35.71	24.31	29.31	29.33	27.74
^{249}Cf	^{207}Pb	^{42}S	110.18	$9/2^-$	$1/2^-*$	4	30.83	32.73	25.67	28.36	28.39	27.49
^{249}Cf	^{201}Pt	^{48}Ca	138.07	$9/2^-$	$(5/2^-)$	2	28.94	33.86	22.86	28.08	28.22	26.38
^{251}Cf	^{205}Hg	^{46}Ar	126.51	$1/2^+$	$1/2^-*$	1	27.54	31.73	21.66	26.99	26.86	24.93
^{232}Pa	^{204}Au	^{28}Mg	71.93	(2^-)	(2^-)	0	26.68	26.51	26.72	25.96	27.29	27.32
^{236}Np	^{208}Tl	^{28}Mg	75.37	(6^-)	5^+	1	25.25	24.95	24.66	24.38	25.77	24.90
^{236}Np	^{206}Tl	^{30}Mg	74.75	(6^-)	0^-*	6	28.59	27.34	26.54	25.95	26.84	27.58
^{238}Am	^{210}Bi	^{28}Mg	78.47	1^+	1^-*	1	24.10	23.93	23.33	22.84	24.94	24.15
^{238}Am	^{206}Tl	^{32}Si	95.03	1^+	0^-*	1	21.97	23.30	20.77	22.12	23.76	22.73

Funding Information Open access funding provided by The Science, Technology & Innovation Funding Authority (STDF) in cooperation with The Egyptian Knowledge Bank (EKB).

Data Availability Statement This manuscript has no associated data or the data will not be deposited. [Authors' comment: Any data that support the findings of this study are included in this published article.]

References

1. G.G. Adamian, N.V. Antonenko, Eur. Phys. J. A **58**, 111 (2022)
2. M. Ismail, A.Y. Ellithi, A. Adel, M.A. Abbas, Phys. Scr. **97**, 075303 (2022)
3. K. Siwek-Wilczyńska, T. Cap, M. Kowal, Phys. Rev. C **99**, 054603 (2019)
4. M. Ismail, A. Adel, Phys. Rev. C **101**, 024607 (2020)
5. M. Ismail, A. Adel, Int. J. Mod. Phys. E **29**, 2050065 (2020)
6. A. Adel, T. Alharbi, Braz. J. Phys. **50**, 454 (2020)
7. K. Santhosh, C. Nithya, At. Data Nucl. Data Tables **119**, 33 (2018)
8. K. Santhosh, C. Nithya, At. Data Nucl. Data Tables **121–122**, 216 (2018)
9. Y.T. Oganessian, A. Sobiczewski, G.M. Ter-Akopian, Phys. Scr. **92**, 023003 (2017)
10. M. Ismail, A.Y. Ellithi, A. Adel, H. Anwer, Chin. Phys. C **40**, 124102 (2016)
11. M. Ismail, A.Y. Ellithi, A. Adel, H. Anwer, J. Phys. G Nucl. Part. Phys. **43**, 015101 (2015)
12. Y.T. Oganessian, V.K. Utyonkov, Nucl. Phys. A **944**, 62 (2015)
13. Y.T. Oganessian, V.K. Utyonkov, Rep. Prog. Phys. **78**, 036301 (2015)
14. K. Morita, Nucl. Phys. A **944**, 30 (2015). (**special Issue on Superheavy Elements**)
15. Y.T. Oganessian, K.P. Rykaczewski, Phys. Today **68**, 32 (2015). https://doi.org/10.1063/PT.3.2880
16. J. Hamilton, S. Hofmann, Y. Oganessian, Annu. Rev. Nucl. Part. Sci. **63**, 383 (2013). https://doi.org/10.1146/annurev-nucl-102912-144535
17. Y.T. Oganessian, F.S. Abdullin, P.D. Bailey, D.E. Benker, M.E. Bennett, S.N. Dmitriev, J.G. Ezold, J.H. Hamilton, R.A. Henderson, M.G. Itkis, Y.V. Lobanov, A.N. Mezentsev, K.J. Moody, S.L. Nelson, A.N. Polyakov, C.E. Porter, A.V. Ramayya, F.D. Riley, J.B. Roberto, M.A. Ryabinin, K.P. Rykaczewski, R.N. Sagaidak, D.A. Shaughnessy, I.V. Shirokovsky, M.A. Stoyer, V.G. Subbotin, R. Sudowe, A.M. Sukhov, R. Taylor, Y.S. Tsyganov, V.K. Utyonkov, A.A. Voinov, G.K. Vostokin, P.A. Wilk, Phys. Rev. C **83**, 054315 (2011)
18. Y.T. Oganessian, F.S. Abdullin, P.D. Bailey, D.E. Benker, M.E. Bennett, S.N. Dmitriev, J.G. Ezold, J.H. Hamilton, R.A. Henderson, M.G. Itkis, Y.V. Lobanov, A.N. Mezentsev, K.J. Moody, S.L. Nelson, A.N. Polyakov, C.E. Porter, A.V. Ramayya, F.D. Riley, J.B. Roberto, M.A. Ryabinin, K.P. Rykaczewski, R.N. Sagaidak, D.A. Shaughnessy, I.V. Shirokovsky, M.A. Stoyer, V.G. Subbotin, R. Sudowe, A.M. Sukhov, Y.S. Tsyganov, V.K. Utyonkov, A.A. Voinov, G.K. Vostokin, P.A. Wilk, Phys. Rev. Lett. **104**, 142502 (2010)
19. S. Hofmann, G. Münzenberg, Rev. Mod. Phys. **72**, 733 (2000)
20. D. Ackermann, Nucl. Phys. A **787**, 353 (2007) (**proceedings of the Ninth International Conference on Nucleus-Nucleus Collisions**)
21. Y. Oganessian, J. Phys. G Nucl. Part. Phys. **34**, R165 (2007)
22. J. Khuyagbaatar, A. Yakushev, C.E. Düllmann, D. Ackermann, L.-L. Andersson, M. Asai, M. Block, R.A. Boll, H. Brand, D.M. Cox, M. Dasgupta, X. Derkx, A. Di Nitto, K. Eberhardt, J. Even, M. Evers, C. Fahlander, U. Forsberg, J.M. Gates, N. Gharibyan, P. Golubev, K.E. Gregorich, J.H. Hamilton, W. Hartmann, R.-D. Herzberg, F.P. Heßberger, D.J. Hinde, J. Hoffmann, R. Hollinger, A. Hübner, E. Jäger, B. Kindler, J.V. Kratz, J. Krier, N. Kurz, M. Laatiaoui, S. Lahiri, R. Lang, B. Lommel, M. Maiti, K. Miernik, S. Minami, A.K. Mistry, C. Mokry, H. Nitsche, J.P. Omtvedt, G.K. Pang, P. Papadakis, D. Renisch, J.B. Roberto, D. Rudolph, J. Runke, K.P. Rykaczewski, L.G. Sarmiento, M. Schädel, B. Schausten, A. Semchenkov, D.A. Shaughnessy, P. Steinegger, J. Steiner, E.E. Tereshatov, P. Thörle-Pospiech, K. Tinschert, T. Torres De Heidenreich, N. Trautmann, A. Türler, J. Uusitalo, M. Wegrzecki, N. Wiehl, S.M. Van Cleve, V. Yakusheva, Phys. Rev. C **102**, 064602 (2020)
23. S. Hofmann, S. Heinz, R. Mann, J. Maurer, G. Münzenberg, S. Antalic, W. Barth, H.G. Burkhard, L. Dahl, K. Eberhardt, R. Grzywacz, J.H. Hamilton, R.A. Henderson, J.M. Kenneally, B. Kindler, I. Kojouharov, R. Lang, B. Lommel, K. Miernik, D. Miller, K.J. Moody, K. Morita, K. Nishio, A.G. Popeko, J.B. Roberto, J. Runke, K.P. Rykaczewski, S. Saro, C. Scheidenberger, H.J. Schätt, D.A. Shaughnessy, M.A. Stoyer, P. Thörle-Pospiech, K. Tinschert, N. Trautmann, J. Uusitalo, A.V. Yeremin, Eur. Phys. J. A **52**, 180 (2016)
24. Y.T. Oganessian, V.K. Utyonkov, Y.V. Lobanov, F.S. Abdullin, A.N. Polyakov, R.N. Sagaidak, I.V. Shirokovsky, Y.S. Tsyganov, A.A. Voinov, A.N. Mezentsev, V.G. Subbotin, A.M. Sukhov, K. Subotic, V.I. Zagrebaev, S.N. Dmitriev, R.A. Henderson, K.J. Moody, J.M. Kenneally, J.H. Landrum, D.A. Shaughnessy, M.A. Stoyer, N.J. Stoyer, P.A. Wilk, Phys. Rev. C **79**, 024603 (2009)
25. D.N. Poenaru, I.-H. Plonski, W. Greiner, 4 Phys. Rev. C **74**, 014312 (2006)
26. M. Ismail, A. Adel, J. Phys. G Nucl. Part. Phys. **46**, 075105 (2019)
27. D.N. Poenaru, R.A. Gherghescu, W. Greiner, Phys. Rev. Lett. **107**, 062503 (2011)
28. D.N. Poenaru, R.A. Gherghescu, W. Greiner, Phys. Rev. C **85**, 034615 (2012)
29. D.N. Poenaru, H. Stöcker, R.A. Gherghescu, Eur. Phys. J. A **54**, 14 (2018)
30. A. Adel, T. Alharbi, Nucl. Phys. A **958**, 187 (2017)
31. K.P. Santhosh, T.A. Jose, Phys. Rev. C **99**, 064604 (2019)
32. X.J. Bao, H.F. Zhang, B.S. Hu, G. Royer, J.Q. Li, J. Phys. G Nucl. Part. Phys. **39**, 095103 (2012)
33. D.N. Poenaru, R.A. Gherghescu, W. Greiner, J. Phys. G Nucl. Part. Phys. **39**, 015105 (2011)
34. Y. Qian, Z. Ren, D. Ni, Phys. Rev. C **94**, 024315 (2016)
35. G. Royer, R. Moustabchir, Nucl. Phys. A **683**, 182 (2001)
36. H.F. Zhang, G. Royer, Phys. Rev. C **76**, 047304 (2007)
37. D. Ni, Z. Ren, Phys. Rev. C **82**, 024311 (2010)
38. M. Ismail, A. Adel, Phys. Rev. C **97**, 044301 (2018)
39. D.N. Poenaru, R.A. Gherghescu, Euro. Phys. Lett. **124**, 52001 (2018)
40. K.P. Santhosh, R.K. Biju, S. Sahadevan, Nucl. Phys. A **838**, 38 (2010)

41. K.P. Santhosh, B. Priyanka, M.S. Unnikrishnan, Nucl. Phys. A **889**, 29 (2012)
42. C. Qi, R. Liotta, R. Wyss, Prog. Part. Nucl. Phys. **105**, 214 (2019)
43. M. Warda, L.M. Robledo, Phys. Rev. C **84**, 044608 (2011)
44. F. Mercier, J. Zhao, R.-D. Lasseri, J.-P. Ebran, E. Khan, T. Nikšić, D. Vretenar, Phys. Rev. C **102**, 011301 (2020)
45. M. Mirea, Eur. Phys. J. A **56**, 151 (2020)
46. C. Xu, G. Röpke, P. Schuck, Z. Ren, Y. Funaki, H. Horiuchi, A. Tohsaki, T. Yamada, B. Zhou, Phys. Rev. C **95**, 061306 (2017)
47. S. Yang, C. Xu, G. Röpke, P. Schuck, Z. Ren, Y. Funaki, H. Horiuchi, A. Tohsaki, T. Yamada, B. Zhou, Phys. Rev. C **101**, 024316 (2020)
48. S. Yang, C. Xu, G. Röpke, Phys. Rev. C **104**, 034302 (2021)
49. K. Uzawa, K. Hagino, K. Yoshida, Phys. Rev. C **105**, 034326 (2022)
50. A. Soylu, C. Qi, Nucl. Phys. A **1013**, 122221 (2021)
51. G. Saxena, P.K. Sharma, P. Saxena, J. Phys. G Nucl. Part. Phys. **48**, 055103 (2021)
52. J.-G. Deng, H.-F. Zhang, G. Royer, Phys. Rev. C **101**, 034307 (2020)
53. D.T. Akrawy, H. Hassanabadi, S.S. Hosseini, K.P. Santhosh, Int. J. Mod. Phys. E **28**, 1950075 (2019). https://doi.org/10.1142/S0218301319500757
54. D.T. Akrawy, H. Hassanabadi, Y. Qian, K. Santhosh, Nucl. Phys. A **983**, 310 (2019)
55. D.T. Akrawy, A.H. Ahmed, Int. J. Mod. Phys. E **27**, 1850068 (2018). https://doi.org/10.1142/S0218301318500684
56. H.C. Manjunatha, K.N. Sridhar, Eur. Phys. J. A **53**, 156 (2017)
57. B. Sahu, R. Paira, B. Rath, Nucl. Phys. A **908**, 40 (2013)
58. S. Zhang, Y. Zhang, J. Cui, Y. Wang, Phys. Rev. C **95**, 014311 (2017)
59. Y. Wang, F. Xing, Y. Xiao, J. Gu, Chin. Phys. C **45**, 044111 (2021)
60. D.N. Poenaru, R.A. Gherghescu, W. Greiner, Phys. Rev. C **83**, 014601 (2011)
61. C. Qi, F.R. Xu, R.J. Liotta, R. Wyss, Phys. Rev. Lett. **103**, 072501 (2009)
62. C. Qi, F.R. Xu, R.J. Liotta, R. Wyss, M.Y. Zhang, C. Asawatangtrakuldee, D. Hu, Phys. Rev. C **80**, 044326 (2009)
63. C. Qi, D.S. Delion, R.J. Liotta, R. Wyss, Phys. Rev. C **85**, 011303 (2012)
64. Z. Ren, C. Xu, Z. Wang, Phys. Rev. C **70**, 034304 (2004)
65. D. Ni, Z. Ren, T. Dong, C. Xu, Phys. Rev. C **78**, 044310 (2008)
66. F. Kondev, M. Wang, W. Huang, S. Naimi, G. Audi, Chin. Phys. C **45**, 030001 (2021)
67. M. Wang, W. Huang, F. Kondev, G. Audi, S. Naimi, Chin. Phys. C **45**, 030003 (2021)
68. V.Y. Denisov, A.A. Khudenko, Phys. Rev. C **79**, 054614 (2009)
69. P. Möller, A.J. Sierk, T. Ichikawa, H. Sagawa, At. Data Nucl. Data Tables **109–110**, 1 (2016)
70. M. Ismail, A. Adel, J. Phys. G Nucl. Part. Phys. **49**, 075102 (2022)
71. M. Bender, K. Rutz, P.-G. Reinhard, J.A. Maruhn, W. Greiner, Phys. Rev. C **60**, 034304 (1999)
72. H. Nakada, K. Sugiura, Prog. Theor. Exp. Phys. **2014**, 033D02 (2014)
73. M. Ismail, W.M. Seif, A. Adel, A. Abdurrahman, Nucl. Phys. A **958**, 202 (2017)
74. M. Ismail, A.Y. Ellithi, M.M. Botros, A. Adel, Phys. Rev. C **81**, 024602 (2010)
75. V.Y. Denisov, Phys. At. Nucl. **70**, 244 (2007)